Physical Basis of Nonequilibrium Solute Transport in Soil

D. A. Barry* and L. Li. *Department of Environmental Engineering, Centre for Water Research, University of Western Australia, Nedlands 6009 Western Australia.*

Abstract

Nonequilibrium solute transport results from both chemical and physical mechanisms. In saturated porous media the physical causes are usually taken to be film diffusion and intra-particle diffusion. Experimental data shows that nonequilibrium is affected by flow velocity, a dependence which would not be inferred from the diffusion-based mechanisms listed. Dimensional analysis of a tracer moving in a porous medium leads to various Damköhler numbers which, in turn, suggest different physical causes of nonequilibrium. It is concluded that both diffusion/dispersion and local variations in the soil-water flow velocity lead to the velocity dependence observed in laboratory experiments. Based on the dimensional analysis, it is also shown that small scale physical modelling of a full scale prototype is feasible under certain conditions. For unsaturated flow, the situation is more complicated in that additional mechanisms, funnelling and fingering, affecting the soil-water flow come into play. These mechanisms are described in some detail, as is experimental data on their occurrence. Commonly, models of solute transport through the unsaturated zone rely on the assumption of steady flow. Then, funnelling and fingering will act as additional physical mechanisms leading to nonequilibrium solute transport.

Introduction

Contaminants can move through soils as either separate liquid or gaseous phases, or as components within phases. There has been considerable research effort aimed at understanding, predicting and ameliorating pollution due to all types of contamination, a common type being that due to NAPLs (e.g., 1-5). Large volume NAPL losses to the subsurface zone have occurred in and around refineries, and from underground storage tanks. Recovery of petroleum products by direct pumping is possible for NAPLs that are less dense than water. However, trapped residual will be left behind in the soil profile. Because industrial processes have been around for a lot longer than environmental awareness, it is common to find that waste chemicals have been dumped into the soil over many years in industrial areas. Chlorinated hydrocarbons like trichloroethylene (TCE) and tetrachloroethylene (PCE) have many industrial uses, e.g., as solvents. In unsaturated soils, these chemicals will volatilise and sorb to organic material. Within an aquifer, they will sorb to organic matter, although the amount of the latter will usually be low. Both TCE and PCE are relatively immiscible with water. They do, however, have solubilities that lead to water degradation. Again, this residual material, even in relatively small volumes, nevertheless acts as a long term source of pollution due to its low aqueous solubility.

Clearly, separate liquid phase or gaseous phase contaminant transport does occur. However, in the case of environmental pollution it is the movement of the water which is frequently of overriding importance. This holds whether immiscible or slightly miscible phases are present, or if chemical species dissolved in the aqueous phase are being transported. In natural porous media dissolved chemical species encounter large solid phase surface areas. Thus, reactions with the solid phase

(sorption), as well as other dissolved species, must be considered. The natural heterogeneity of porous media renders both the type of reaction site and the spatial distributions of sites subject to uncertainty. More generally, the natural variability of soil profiles leads to uncertainty in attempts to predict chemical transport processes. It is usually not possible to model with much precision the heterogeneous physical and chemical characteristics of the soil nor, in most cases, is such detail of any interest in practice. For example, it is often of more interest to estimate the rate at which a dissolved chemical enters an aquifer from the unsaturated zone or passes a given plane within an aquifer. One approach is to estimate the effective properties of the medium at the scale of interest.

How are these effective properties to be estimated reliably? Typically, soil samples are collected and laboratory experiments are carried out. The experimental data are analysed using a mathematical model in which the model parameters are determined by a combination of fitting and independent experiments. These parameters are then used in the same model or as part of some larger (e.g., catchment) model to make predictions upon which management decisions are based. Are the laboratory-based parameters appropriate in making predictions at the larger, prototype scale? Apart from the question of scale changes, other differences could be considered. In particular, even though the same soil has been used, the natural flow conditions are unlikely to be replicated. Aspects of these issues will be discussed below in more detail.

The question of scale cannot be divorced from considerations of whether model simplifications are appropriate. For example, long term contaminant leakage from a landfill through 10 metres of the vadose zone to an aquifer is quite different from catchment wide nutrient loading of an aquifer as a result of non-point source pollution, even though the landfill may lie within same catchment. The consideration of scale is further complicated by the type of chemicals being transported. The landfill may contain persistent organics or heavy metals, while at the catchment scale nutrients like phosphates or nitrates are often of more concern. Predictions of solute movement at the local scale (<< catchment scale) rely on knowledge of the local transport mechanisms, and below it is mainly this scale that is considered.

The heterogeneity of natural soils imposes uncertainty in the water flow field and the types of reactions dissolved solutes may undergo. The former is parameterised as the variability of the hydraulic conductivity, K (a complete notation list is included at the end of the paper), while parameterisation of the latter depends on the type of reaction. Perhaps the most simple case is that of a single species, ion exchange process characterised by a spatially variable retardation coefficient, R. These parameters may be correlated with each other via, e.g., the clay content of the soil. In more complicated solute reaction scenarios, there are many more parameters involved. Although sophisticated models coupling reaction and transport have been developed (e.g., 6-9), it is likely that such models will be useful most often in research applications due to the numerous parameters that must be known prior to simulation.

A more pragmatic modelling approach is followed here, that of nonequilibrium solute transport models. The most simple nonequilibrium transport model is that for a nonreactive tracer. In addition to the usual dispersion and flow velocity parameters, there is an additional nonequilibrium rate parameter. There is ample evidence that this single additional parameter produces a model that is sufficient to describe most experimental data sets, at a variety of scales. However, we show that physical explanations of this parameter are somewhat unsatisfactory, and do not permit laboratory-based results to be transferred to larger scales.

Another type of uncertainty is due to uncertainty in boundary and initial conditions. Before any modelling approach can be implemented, it is necessary to have detailed knowledge of the initial distribution of, e.g., water pressure heads. Further, boundary condition uncertainty can lead to gross under- or over-estimation of water and solute transport. For example, vadose zone flow and transport is markedly affected under some circumstances by periodicity in the surface recharge and near-surface hysteretic water flow (10-12).

For applications, it is neither practical or desirable to monitor the physical system and boundary conditions to the extent necessary to predict in detail every transport process that is occurring. For this reason, it is useful, again, to adopt a pragmatic, or phenomenological, approach to solute transport modelling. As indicated, nonequilibrium models fall into this category. The approach taken is based on the assumption that the flow of water is the dominant mechanism for transporting solutes, and that local variability of the water flow is responsible for solute spreading. Discussion will focus on the physical processes controlling the solute transport, on the presumption that physical heterogeneity controlling the flow outweighs heterogeneity of the chemical reactions that may occur. In addition, no detailed mathematical models will be developed. Rather, the nonequilibrium transport processes are considered in the light of dimensionless variables inherent in the problem. Finally, we discuss briefly possible causes of nonequilibrium in unsaturated zone transport.

Saturated Water Flow and Solute Transport

Chemical Nonequilibrium

For saturated soil the governing steady flow model is (e.g., 13)

$$\nabla . (K \nabla \phi) = 0, \tag{1}$$

where the hydraulic conductivity, K, varies with position. Solving the flow equation, Eq. (1), with appropriate boundary conditions gives the piezometric head, ϕ, from which the local groundwater flux, $\mathbf{q}$, can be calculated from Darcy's law. The flux vector is used in the governing solute transport equation (e.g., 14)

$$\frac{\partial [\theta (c + s)]}{\partial t} = \nabla . (\theta D \nabla c - \mathbf{q} c) \tag{2}$$

where c is the solute concentration in the fluid phase, s is the solid phase concentration (in liquid phase concentration units) and there are no sources or sinks of solute within the medium. In Eq. (2) only a single solute species has been assumed. The quantity $s + c$ represents the total solute mass in the solid and liquid portions of the porous medium, while the terms on the right hand side model the diffusion/dispersion and advection of solute within the liquid phase. Multispecies models can be written; but for consideration of the physical properties of nonequilibrium transport, a single species is sufficient. Note that Eqs. (1) and (2) are coupled through the density changes induced by the dissolved species. It is assumed here that the concentration is dilute and that the density coupling can be ignored. An additional equation for s is needed to solve Eq. (2). If the sorption to the solid phase is instantaneous, then

$$s = f(c), \tag{3}$$

where f is a sorption isotherm, e.g., the Freundlich, Langmuir or S-curve isotherms (e.g., 7, 15). If

Eq. (3) applies, then the soil and liquid phase solute concentrations are always in equilibrium. On the other hand, if the sorption is time dependent, then Eq. (3) is replaced by a rate equation, e.g.,

$$\frac{\partial s}{\partial t} = \alpha [f(c) - s], \tag{4}$$

where α is the "reaction rate". Equation (3) is a special case of Eq. (4) resulting for $\alpha \rightarrow \infty$. Setting $\alpha = 0$ in Eq. (4) reduces Eq. (2) to a tracer transport model.

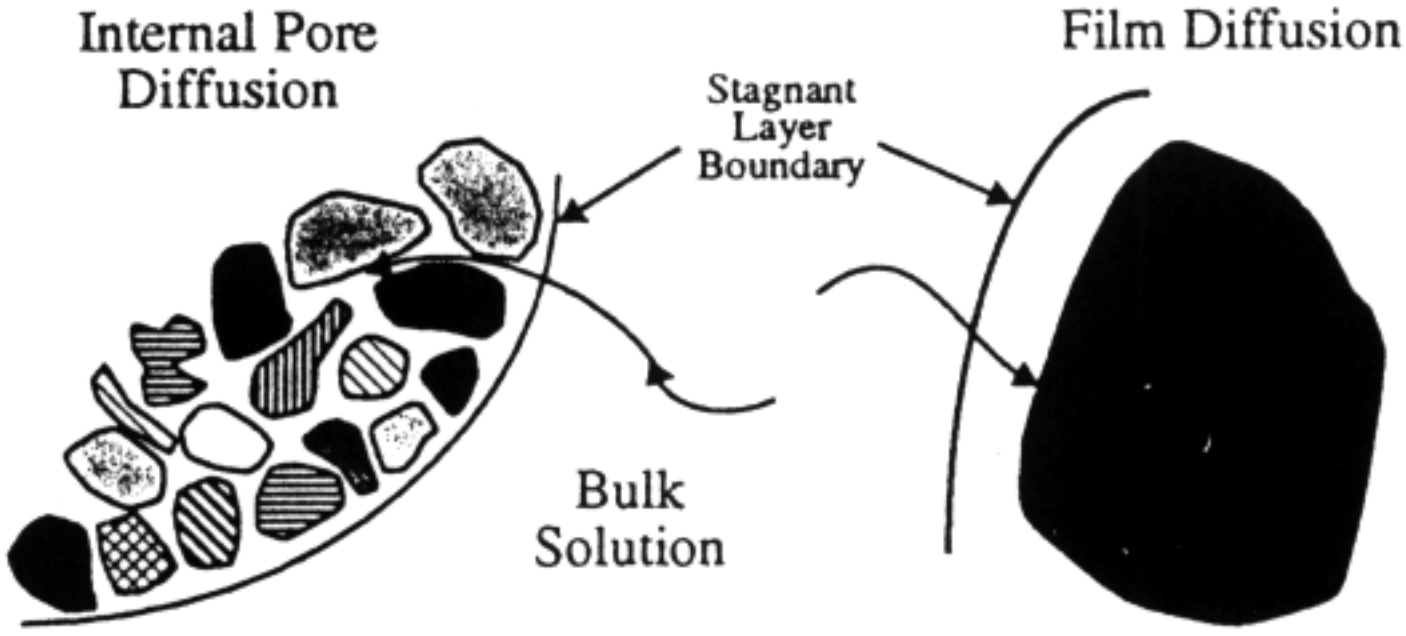

Figure 1. Schematic diagram showing the internal pore diffusion and surface film diffusion concepts. For internal pore diffusion, solute migrates from the bulk solution into soil aggregates to reach a sorption site within, whereas for film diffusion only the stagnant layer attached to the soil grain surface limits the reaction rate.

The nonequilibrium rate parameter, α, has been conceptualised in different ways (e.g., 16). For ion-exchange reactions on soil particles, α is affected mainly by three processes: (i) the time-dependent reaction at the exchange site, (ii) film diffusion and (iii) internal pore or intra-particle diffusion. The latter two processes are physical, rather than chemical, but they are mentioned here for convenience because they occur at the scale of the soil aggregate, or less. In Figure 1 the film diffusion and intra-particle (or internal pore) diffusion mechanisms are displayed. These mechanisms (and detailed discussions on their effect on solute adsorption) are given elsewhere (e.g., 17-19).

Although Eqs. (3) and (4) can be derived for certain simple systems, they are best considered as phenomenological equations. It is not difficult to extend the basic transport model presented here. A popular choice is to assume that there are two different types of sorption sites available in the soil. On some volume fraction of the soil equilibrium reactions occur, with rate-limited reactions taking place elsewhere. Clearly, the fraction of sites becomes another parameter in this so-called "two-site" model (20, 21). Of interest, however, is that diffusion is the most likely controlling mechanism in "chemical" nonequilibrium.

Physical Nonequilibrium

Classical physical nonequilibrium occurs when a tracer encounters two different flow regimes in the soil, a mobile region where advection and diffusion/dispersion occur and an immobile where diffusion alone occurs (22). Equation (1) still holds for the piezometric head, while Eqs. (2) and (4)

become, respectively,

$$\frac{\partial(c_m\theta_m + c_{im}\theta_{im})}{\partial t} = \nabla.(\theta_m D\nabla c - \mathbf{q}c) \tag{5}$$

and

$$\frac{\partial(c_{im}\theta_{im})}{\partial t} = \alpha(c_m - c_{im}). \tag{6}$$

Here; α is the mass transfer rate between the mobile and immobile regions. Equation (6) is somewhat different from the corresponding equation presented by Russo et al. (12), who consider the transfer rate to be proportional to the concentration difference in units of solute mass per unit volume (of soil and soil water). However, Eq. (6), which assumes the transfer rate to be proportional to the difference between the solute concentrations in the two regions, is more reasonable and widespread in the literature (e.g., 18). Again, the model consisting of Eqs. (5) and (6) can be modified to account for, say, equilibrium solute sorption. Under appropriate conditions (uniform flow, linear sorption isotherm, constant θ_m and θ_{im}, etc.), the one dimensional form of Eqs. (2) and (4) is mathematically identical to Eqs. (5) and (6) (23, 24).

Like the intra-particle and film diffusion concepts discussed above, the mobile-immobile region model is appropriately termed physical nonequilibrium. The (somewhat artificial) distinction is made that in this model there is no chemical reaction occurring; the effect is purely physical. Clearly, the model of a soil with "mobile" and "immobile" zones will break down except, perhaps, in certain specialised situations like aggregated soils. But, there is ample evidence that models like Eqs. (5) and (6) have proved remarkably versatile. The key parameter is the mass transfer rate, α. As an apparent parameter, its meaning will change according to the physical characteristics of the transport problem. However, in order to transfer results from one situation to another, the meaning of α and similar parameters should have some physical basis. Below, possibilities are examined in conjunction with dimensional analysis.

Table 1. Parameters and length scales affecting physical nonequilibrium solute transport models.

Property	Symbol	Dimensions
Dispersion Coefficient	D	L^2T^1
Molecular Diffusion Coefficient	D_m	L^2T^1
Apparent Reaction/Transfer Rate	α	T^1
Pore Water Velocity	v	LT^1
Local Length Scale	l	L
Macroscopic Length Scale	L	L

Dimensional Analysis of Nonequilibrium Solute Transport

The different meanings for the transfer/reaction rate parameter, α, in Eqs. (4) and (6) are best differentiated by the physical and chemical processes affecting the solute. The conceptual models outlined in Figure 1, however, are, at best, idealised representations of the heterogeneous nature of soil material and structure (and hence pore spaces within the soil). It is possible, nonetheless, to use dimensional analysis to help characterise and elucidate the nonequilibrium solute transport process.

For the purpose of illustration consider some unknown sorption reaction. It is assumed that there is some characteristic value (or perhaps distribution) for the reaction rate. This can be determined by standard batch experiments. Then, the fundamental parameters that are involved are essentially those contained in, or derived from, Eq. (2), plus appropriate length scales, as listed in Table 1.

Table 2. Dimensionless groups derived from the parameters in Table 1. The quantities below the heavy line are derivable from those above.

Group	Name	Symbol
$\frac{\alpha l}{v}$	Damköhler Group I	Da_I
$\frac{\alpha l^2}{D_m}$	Damköhler Group II	Da_{II}
$\frac{D_m}{D}$	Diffusion/Dispersion ratio	d
$\frac{l}{L}$	Length scale ratio	X
$\frac{vl}{D_m}$	Local Péclet Number	P_l
$\frac{vL}{D}$	Macroscopic Péclet Number	P_L
$\frac{\alpha D}{v^2}$	Damköhler Group III	Da_{III}

The two length scales in Table 1 are L, the macroscopic length scale imposed on the system, e.g., the length of a laboratory column, and l, the local length scale controlling the apparent reaction rate. For the cases in Figure 1, l can be taken as the size of the aggregate for intra-particle diffusion and the stagnant layer thickness for film diffusion. The molecular diffusion coefficient is used rather than the longitudinal dispersion coefficient alone because the conceptual models are clearly based on diffusion processes, as is the mobile-immobile region model. From Table 1 the dimensionless groups in

Table 2 are derived. Note that the Damköhler group number definitions in Table 2 are similar to those given by Boucher and Alves (25). In Table 2 a distinction has been made between local and macroscopic quantities. For the present the appropriate length scales are the pore or grain size scale for the former, and the laboratory column scale for the latter. Clearly, for intra-particle diffusion, the conceptualisations given above (Figure 1) are appropriate at local scales, suggesting that Da_{II} is the appropriate description of the transfer mechanism. In other words, the intra-particle conceptualisation leads to the conclusion that the apparent transfer rate, α, is independent of the mean pore water velocity, v.

Generally, the same considerations lead to Da_{II} being the appropriate dimensionless number describing the film diffusion through a fixed layer. An upper bound for l is the typical pore size in the medium. However, this correspondence will be associated with Da_I if the variation of the stagnant layer thickness with local velocity is taken into account. The local length scale, l, is the layer thickness which would scale as $l \sim \nu/v$, where ν is the kinematic viscosity of soil water. Because the solute must diffuse through the layer, the appropriate dimensionless number is again Da_{II}. We have

$$Da_{II} = \frac{\alpha l^2}{D_m} \sim \frac{\alpha \nu^2}{D_m v^2} = \left(\frac{\alpha}{v}\right)\left(\frac{\nu}{v}\right)\left(\frac{\nu}{D_m}\right), \qquad (7)$$

where the final term in parentheses is nearly constant. Because $\nu/v \sim l$ the right hand side then proportional to Da_I. A somewhat "black-box" conceptualisation of Da_I is shown in Figure 2, in which there are two relevant time scales. Clearly Da_I is the ratio of the advective time scale, t_a, to the reaction time scale, t_r. Some physical attribute of the system must be invoked before the appropriate length scale, l, can be determined. In typical applications of Eqs. (5) and (6) l is replaced by the macroscopic length scale, L. In such cases the soil is treated as an unknown system. If nonequilibrium effects are observed in a soil sample of length L, i.e., $t_a \approx t_r$; then, if no obvious soil structural causes are evident, a reasonable conclusion is that the variability of the local flow paths is responsible for the observed nonequilibrium effect. Such a mechanism, while not fitting particularly well the conceptual models of Figure 1, is discussed further below.

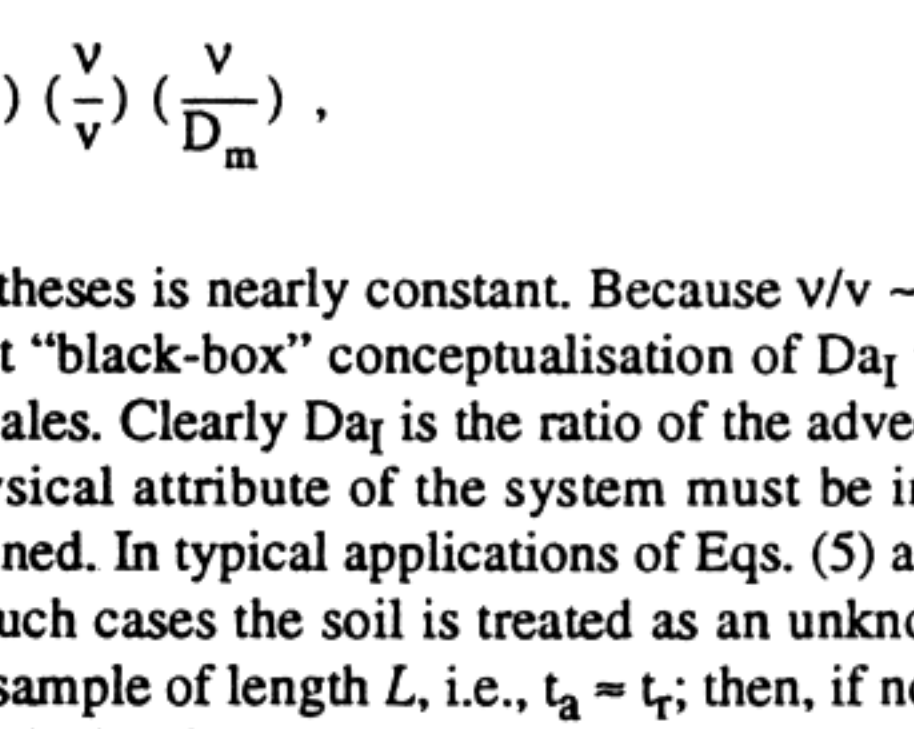

Figure 2. The basis (or lack thereof) of Da_I. Two time scales are shown, t_a, the advection time scale and t_r, the reaction time scale.

For the conceptual models presented in Figure 1 typical time scales for α can be calculated. Suppose a laboratory experiment is carried out on a sandy soil with a pore (grain) size of 10^{-4} m at a pore water velocity of 10^{-3} m s^{-1}. Then from Da_I the typical transfer time across the stagnant fluid is 10 s. Because the travel time through the laboratory column is much greater than this, the characteristic tailing of the breakthrough curve (BTC) resulting from nonequilibrium effects should not be observed. Instead, a symmetric BTC will be produced, albeit with a possibly enhanced dispersion coefficient. If, instead, the soil is composed of aggregates with a size of 10^{-2} m, then for $D_m \approx 10^{-9}$ m^2 s^{-1} the transfer time scale is, using Da_{II}, approximately 10^5 s. Nonequilibrium effects acting on this time scale will thus be observed in most laboratory experiments. However, because the nonequilibrium effect in this case is a diffusion-dependent phenomenon, it is independent of the flow velocity.

Flow velocity effects on α have been detected in several independent experiments (26, 27). Processes which follow the Da_{II} scaling cannot show velocity dependence of α. Further, it is clear that film diffusion alone is unlikely to cause the nonequilibrium effects observed in laboratory experiments, and the black-box shown in Figure 2 offers no physical mechanism to explain velocity effects. As the conceptual models discussed above do not allow for velocity dependence, an alternative approach is needed.

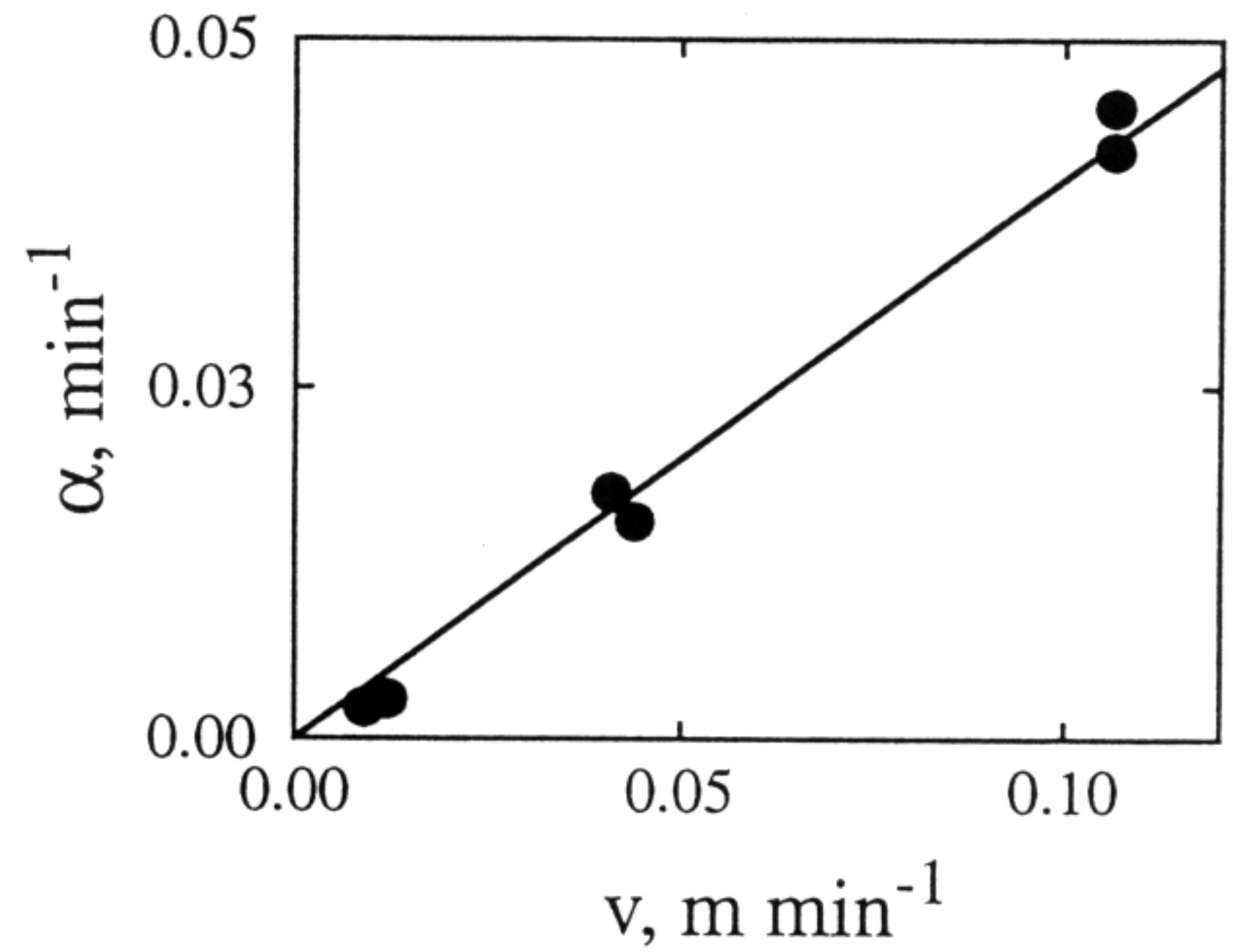

Figure 3. Relationship between apparent reaction rate, α, and the mean pore water velocity, v, deduced by Herr et al. (26) from their laboratory experiments. The solid circles represent the fitted values of α and solid line is a fitted curve with a slope of 0.4 m^{-1}.

Velocity-Dependent Nonequilibrium

Herr et al. (26) reported laboratory experiments carried out using an artificial heterogeneous medium. The porous medium was constructed by taking a uniform sand and randomly placing within it ceramic blocks of various shapes and permeabilities. The ceramic inclusions had a different permeability to the surrounding sand, but were not immobile regions. Nevertheless, the mobile-immobile model was fitted to the BTCs (breakthrough curves), with excellent fits. In addition, they plotted the relationship between α and v for one experimental setup. These data are reproduced in Figure 3, where a linear relationship between α and v is evident. Clearly, Da_I is the appropriate Damköhler number in this case. In addition, a length scale which could be used in Da_I is of the order of the inverse of the slope of the line drawn in Figure 3, about 2.5 m. Unfortunately, this length scale is of the order of the column length and so cannot be related directly to the length scale of the porous ceramic inclusions.

Another study along these lines indicated by has been reported by Li (28). In this case the experiments consisted of tracer transport through a saturated silt soil column within which porous polyethylene segments were placed in fixed proportions. Breakthrough curves from the column experiments were fitted to solutions of the mobile-immobile model given above using a modified version of the CXTFIT code (29). For each experiment, polyethylene segments and silt were mixed. Then, a BTC was generated using an arbitrary initial flow rate. This initial BTC was used to fit the mobile-immobile model parameters. In subsequent experiments, the flow rate was increased. However, in fitting the BTC only v and α were fitted, with previously computed parameters held constant. In all cases the BTC fits were satisfactory. The results of two experimental runs are shown in Figure 4, along with curve fits of the data. Two features in the results are apparent. First, the proportionality between α and v observed in Figure 3 has been replicated. Second, in some experiments the data suggest that α is proportional to v^2, rather than v.

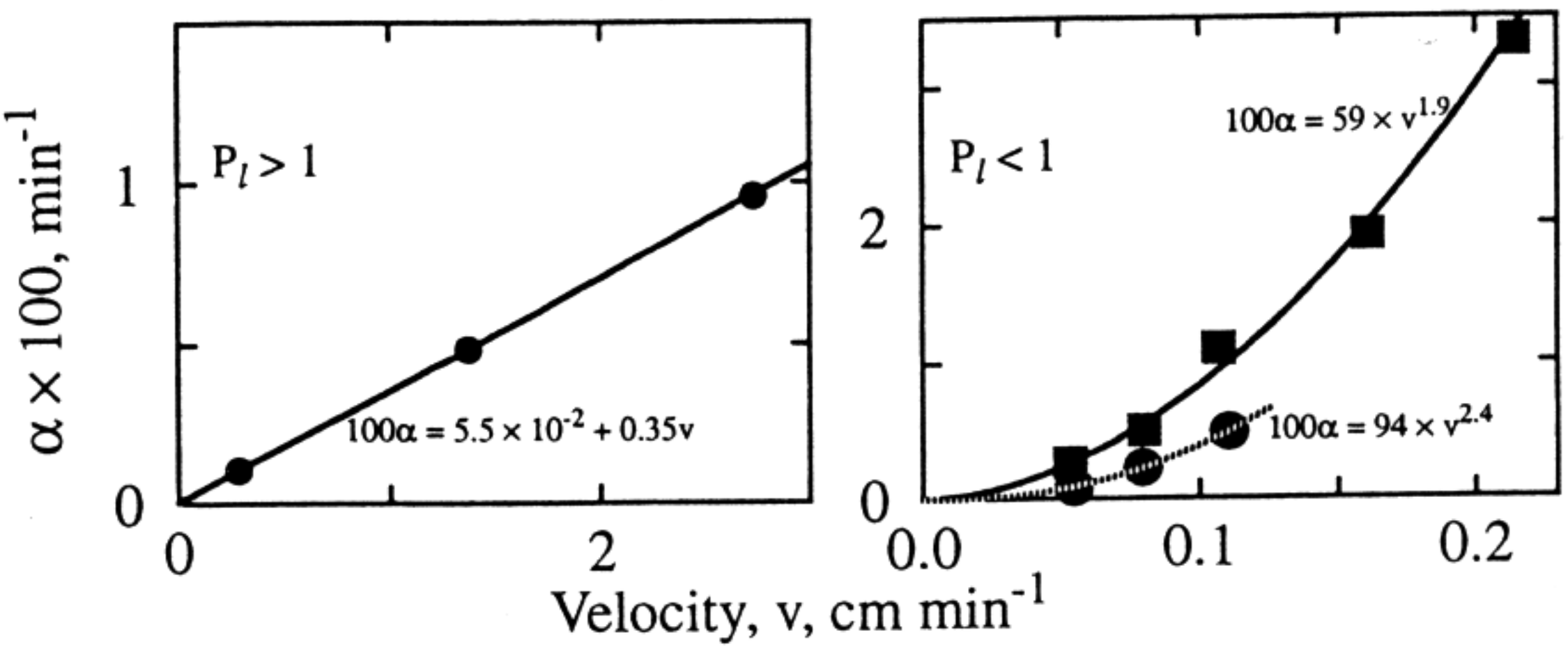

Figure 4. Experimental results from Li (28). In each case the symbols represent data from different soils for different pore-water velocities while the lines represent fitted curves. Each data set was obtained from soil (silt) columns with the following proportions of polyethylene inclusions: small circles - 11%, large circles - 12% and squares - 18%.

Taken as a whole, the data in Figure 4 demonstrate that, in laboratory columns at least, the appropriate scaling for the transfer rate is $\alpha \propto v^2/D$, i.e., Da_{III} will be constant for a given soil. This scaling automatically includes the case of proportionality between α and v. When $P_l > 1$ (l is the typical grain size in this case), the dispersion coefficient, D, is proportional to v (30, 31), or $\alpha \propto v$. In addition, Da_{III} yields $\alpha \propto v^2$ when $P_l < 1$ since then $D \propto D_m$. These results, while they have been obtained using an artificial soil, provide evidence that velocity scaling of the nonequilibrium transfer rate may be given by Da_{III} under certain circumstances. Velocity scaling according to Da_{III} has a somewhat different conceptual interpretation to the mechanisms proposed in Figure 1. One interpretation is that the length scale, l, in Da_I is of the order of the dispersivity, D/v, in which case Da_I and Da_{III} are identical. Another related interpretation is that there is a nonequilibrium mixing length characteristic of the soil. Such a length would have to be related to the variation of the velocity field. In this conceptualisation, both velocity variations and diffusion/dispersion play a role since the (apparent) transfer rate (α) would increase with the former (which is proportional to v^2), while diffusion/dispersion would act to mix solute between flow paths and so reduce the nonequilibrium mechanism. In other words, the effect of velocity variations is in balance with that of dispersion, i.e., $\alpha \propto v^2/D$.

Connection with Stochastic Solute Transport Theory

Based on the preceding discussion, it is not surprising that there is a close connection between the two-region models and the solute transport models based on the assumption of a random velocity field. Indeed, the mobile-immobile conceptualisation is simply a medium in which there are two different pore water velocities, rather than a range. The case of a tracer moving in a random velocity field is perhaps the most simple as there are no chemical reactions or transformations to be considered. The governing equation is then a simplification of Eq. (2):

$$\frac{\partial c}{\partial t} = \nabla . (D \nabla c) - \mathbf{v} . \nabla c, \tag{8}$$

where steady flow and a uniform moisture content have been assumed, and D is a local dispersion coefficient (possibly a tensor). Sposito and Barry (32) considered the case that **v** is a wide-sense stationary stochastic process, i.e., having uniform mean and a correlation function that depends on differences in position and time alone. Ensemble averaging of Eq. (8) leads to the governing equation for the ensemble-averaged concentration. This equation has the same form as Eq. (8) except that v is replaced by the mean (constant) velocity, and D is replaced by a macrodispersion tensor with time-dependent diagonal elements. From this approach it was shown that the macrodispersion coefficients of, e.g., Gelhar and Axness (33) and Dagan (34), could be derived.

The details of these analyses are not important. An approximation for the general behaviour of the longitudinal time-dependent macrodispersion coefficient, D_L, takes the functional form:

$$D_L = D_l + (D_M - D_l) \left[1 - \exp\left(-\frac{vt}{l_s}\right) \right], \tag{9}$$

where D_l is the local (or laboratory) dispersion coefficient, D_M is the asymptotic value of the field-scale dispersion coefficient, v is the mean pore-water velocity and l_s is the correlation length scale of

the velocity field. Similar models to Eq. (9) can be derived by making use of the well known result (35):

$$D_M = \frac{1}{2}\frac{dVar(X)}{dt} = \sigma_v^2 \int_0^t A(\bar{t})\, d\bar{t}, \tag{10}$$

where X is the position of a tracer particle moving in the flow field, D_M is now time dependent and A(t) is the autocorrelation function for the particle. The time dependent part of Eq. (9) results from Eq. (10) if A(t) is proportional to $\exp(-vt/l_s)$.

Equation (9) is usually not an exact result. Rather, it displays the characteristic increase with time of the dispersion coefficient, as well as the time scale for the increase, that is predicted by the ensemble averaging procedure. Thus, for time scales $t >> l_s/v$ the asymptotic dispersion coefficient is obtained from Eq. (9).

Spatial moments can be calculated for tracer transport using the mobile-immobile region model. In that case an expression is obtained that can be written in a form similar to that of Eq. (9). For illustration, an infinite one-dimensional domain is considered. Taking the one-dimensional version of Eqs. (5) and (6) as the governing model, the effective dispersion coefficient is (28)

$$D_{eff} = \frac{D\theta_m}{\theta_{im}+\theta_m} + \frac{v^2(\theta_m\theta_{im})^2}{\alpha(\theta_m+\theta_{im})^3}\left\{1-\exp\left[-\alpha\left(\frac{1}{\theta_m}+\frac{1}{\theta_{im}}\right)t\right]\right\}. \tag{11}$$

Clearly, Eq. (11) is of the same form as Eq. (9). For a stochastic model that has a dispersion coefficient with generic form of the latter equation, a roughly equivalent representation can be determined using Eq. (11), the parameters of which become fitting constants. In other words, because the dispersion coefficient is closely related to the variance of a solute plume, the mobile-immobile transport model will reproduce the dispersion observed by a plume at the field scale at which Eq. (9) applies. This type of relationship between models is discussed elsewhere (36). For the present, it is the scaling $\alpha \sim v/l_s$ implied by Eqs. (9) and (11) which is of interest. Note that, if l_s is constant, using this scaling means that the dispersion coefficient in Eq. (5) does not vary with time or, equivalently, position if steady flow is considered.

Numerous experiments have shown that, in the field, the apparent dispersion coefficient increases with the observation scale. A recent compendium of the available field data was presented recently by Gelhar et al. (37) where this trend was observed, although the reliability of very large scale dispersivities is not great. These data suggest that the length scale, l_s, in Eq. (9) depends on the observation scale, and hence that the apparent nonequilibrium effect will be persistent. Clearly, l_s has little to do with the conceptual models of Figure 1. It is, however, consistent with the black-box approach shown in Figure 2. It is possible to treat l_s as a scale dependent dispersivity, in which case Da_I reduces to Da_{III}.

A standard engineering design method is to analyse the behaviour of a full scale prototype using a small scale laboratory model. The possibility of physical modelling of the prototype depends on whether appropriate force, time and length scales can be maintained in the scale model. If an exact scaling is feasible then the results from the laboratory model can be directly scaled to the prototype without recourse to a mathematical model.

Most laboratory experiments on solute transport in soils reduce the time scale for the process by increasing the flow rate (relative to that of the prototype) through the sample. For two-region transport models such as Eqs. (5) and (6), it has been shown that the main conditions for similarity between model and prototype are that the grain Péclet number, P_l, is less than unity and Da_{III} is constant (28). Note that the P_l restriction sets an upper limit for the flow velocity in the laboratory experiment. If these conditions hold and the velocity in the model (relative to that of the prototype) has been increased by a factor of N, the experimental results apply to a prototype that is N times larger. The time needed to perform a laboratory experiment is N^2 less than a corresponding prototype experiment.

For saturated flow and transport the above discussion indicates that the nonequilibrium effects commonly observed in natural soils are most likely a manifestation of a variable flow field. The scaling of the apparent sorption rate, α, from dimensional analysis will certainly help in estimating model parameters or constructing a physical model for the purpose of predicting contaminant movement in an aquifer. This will remain the case even for reactive transport unless independent (e.g., batch) experiments reveal a relatively slow reaction rate. The question then naturally arises whether similar deductions can apply to unsaturated flow.

Unsaturated Water Flow

Movement of water in the unsaturated zone is a phenomenon affected by both medium heterogeneity and nonlinearity. Furthermore, it is prone to instability, and temporal variability at the soil surface. Two properties are used to model such flows: the soil moisture characteristic curve relating moisture content to soil water capillary pressure and the hydraulic conductivity as a function of moisture content. In heterogeneous media, these two properties will vary with position as well as water content.

Kung (38, 39) reported an experiment where 30 cm of dyed water was added to two 3×3.6 m plots of loamy sand over an 80-day period. The site was excavated, and the dye patterns noted. The significant impact of relatively minor soil textural differences (heterogeneity) on the unsaturated flow pattern was evident. The flow was funnelled by the layering so that, at a depth of 3 m, the percolating fluid passed through only 10% of the soil matrix. This figure reduced to 1% for the 6 m depth. Significant lateral displacement of the dyed liquid was observed also. The funnelling occurred when a soil layer was overlain by a finer grained layer. Water in the finer material will pass into the coarser material only when the difference in capillary suction is overcome. This, of course, is the principle of capillary barriers used to channel subsurface flows.

The results revealed that the effect of the soil layering was significant in that, with increasing depth, the dyed liquid passed through progressively less of the soil matrix. However, a mass balance of the liquid was not attempted and, given that the funnelling could introduce undyed water into the soil

profile from adjacent locations, it is not possible to quantify the accuracy of Kung's estimates of the volume of the soil matrix transmitting the percolating water. Again, the question of scale is relevant. If it is necessary to predict the local behaviour of the infiltrating water, then Kung's experiment, carried out at the scale of a few metres, shows well the effects of local heterogeneity on the unsaturated flow patterns. It does not, however, indicate the possible averaging effects of larger horizontal and vertical scales.

Various other unsaturated zone solute transport experiments have been performed (e.g., 40-42). Quite recent studies using relatively large scale plot sizes have been reported (43-46). These studies were designed to determine the effects of field scale variability on tracer transport. Butters et al. (43) applied a bromide tracer pulse across a 0.64 ha loamy sand field. Like Kung, they observed that the volume of the soil matrix responsible for transporting the applied water reduced with depth below the soil surface. White et al. (47) define the transport volume as the fraction of the wetted pore space through which the solute moves. Butters et al. (43) defined the depth-averaged transport volume as

$$\bar{\theta}(z) = \frac{q}{v_s}, \tag{12}$$

where $\bar{\theta}$ is the depth-averaged porosity, q is the steady water flux and v_s is the mean solute velocity. Both quantities on the right side of Eq. (12) were calculated from the experimental data, with v_s calculated from analysis of solute breakthrough curves at sampling sites within the soil profile. In Figure 5 data from Butters et al. (43) are reproduced along with the simple curve fit:

$$\bar{\theta}(z) = \frac{1.1}{z^{0.3}}. \tag{13}$$

Apart from the value at 30 cm, Eq. (13) fits the experimental data satisfactorily. Although Butters et al. (43) have presented the depth-averaged porosity, the change in the transport volume with depth is somewhat obscured. The definition of depth averaging is

$$\bar{\theta}(z) = \frac{1}{z}\int_0^z \theta(\bar{z})\, d\bar{z}. \tag{14}$$

From Eqs. (13) and (14) the transport volume porosity for the Tujunga loamy sand is approximated by

$$\theta(z) = \frac{0.77}{z^{0.3}}. \tag{15}$$

Equation (15) indicates that between the surface layer (between 0 and 60 cm depth) and the 4.5 m depth, the transport volume through which the solute moves is reduced by a factor of 2. Although this reduction factor is less than that reported by Kung (38), the trend is identical, i.e., with increasing depth the solute is transmitted through smaller proportions of the available soil matrix. Consequently, if it is assumed that the average liquid flux passing through any given depth is constant (i.e., water, on average, does not accumulate within the profile), then the mean velocity of the solute must increase with depth. This is, of course, precisely what was observed, as the data shown in Figure 5 are based on the mean solute travel time.

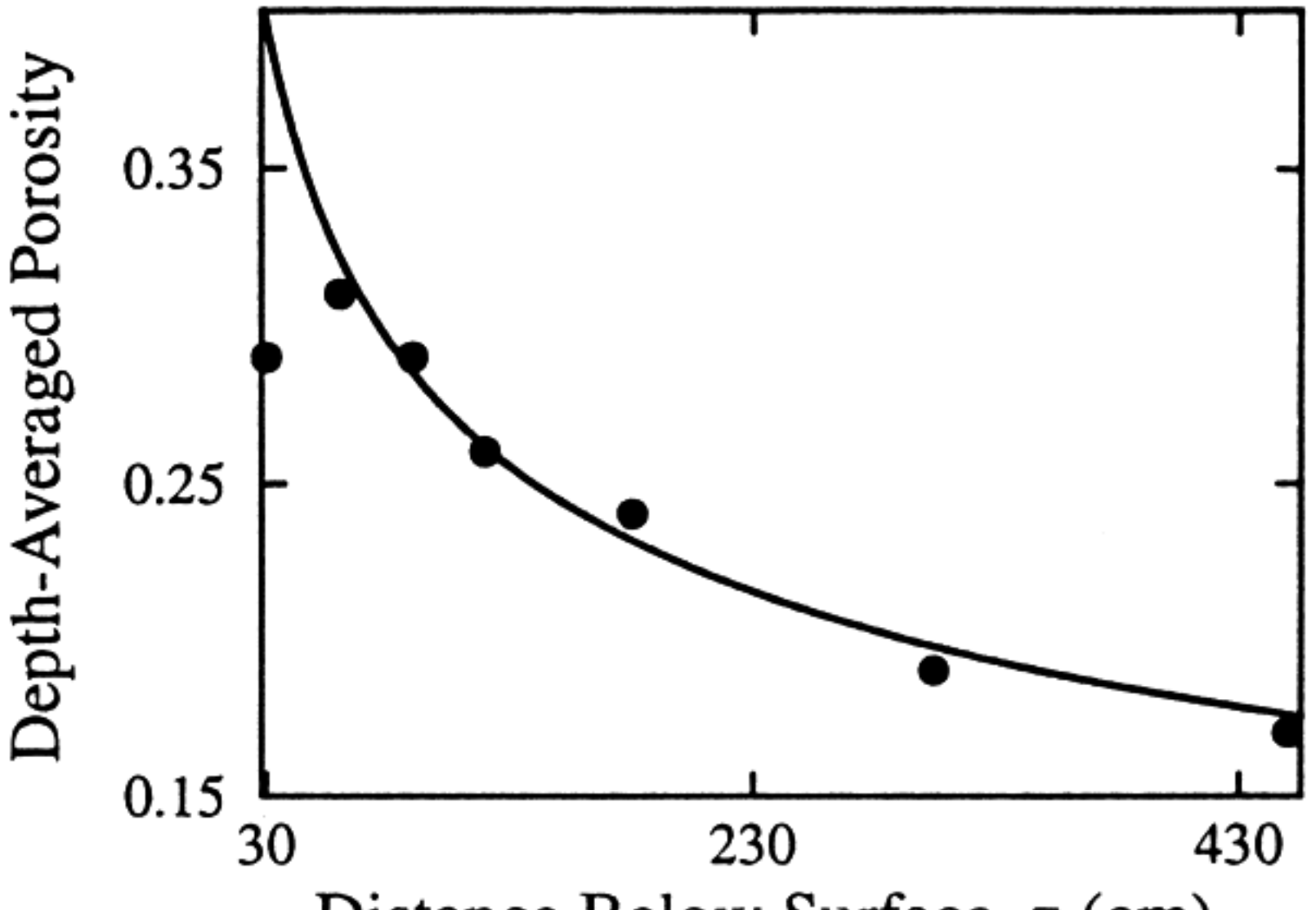

Figure 5. Depth-averaged volumetric water content as a function of depth below the soil surface for the Tujunga loamy sand (43). The line is a fit (by eye) of the data (excluding the value at 30 cm) using Eq. (13).

These experiments show that the available volume of pore space is not utilised by the percolating water. An alternative mechanism to funnelling for this observation is discussed below.

Unstable Flow

Early analyses of unstable flow systems in porous media were provided by Saffman and Taylor (48) and Chuoke et al. (49). Since then, numerous experimental and theoretical studies have been reported (50-64). Fingering, the result of unstable flow, occurs in situations when the hydraulic conductivity of the medium increases with depth. There is considerable experimental evidence for fingering phenomena. Figure 6 shows a typical instability experiment. Water is added (not necessarily ponded) to the surface of a dry soil with a well defined textural interface between the upper (fine) and lower (coarse) layers. Fingers form at the interface and propagate downwards, generally following a vertical path, although splitting and joining of fingers is possible. The interior of the fingers is close to saturation, whereas outside the fingers the soil remains dry. Over time, however, lateral diffusion wets the areas surrounding the fingers. The cores remain very moist and transmit the majority of the water moving through the system. Fingers form even if the soil is initially moist, but they are very broad (60). An increased surface flux also leads to broader fingers (65). Field evidence of fingering has been presented by Starr et al. (66) and Glass et al. (60), who found that fingers persist in the subsurface over length scales of a metre or more.

Funnelling and Fingering

The combination of the experimental evidence reviewed above indicates that both textural heterogeneity (leading to funnelling) and instability (giving rise to fingering) play a role in transporting solutes in the vadose zone. Relative to the saturated zone, heterogeneity in the unsaturated zone will

have a greater influence on water movement. The theoretical and laboratory data on fingering show that the conditions for instability are predictable, and that the individual finger properties and behaviour can be quantified. Funnelling will occur when unsaturated moisture flow, either in the form of a finger or a uniform front, encounters a sloping coarse layer. The funnelling will continue until the layer finishes or another finger is produced due to instability at the interface. The heterogeneity in even relatively uniform natural media will both promote fingering and attenuate it by the funnelling mechanism. With increasing initial moisture content these effects will be diminished as the fingers broaden and the funnelling is reduced. However, the laboratory experiments of Diment and Watson (59) and Glass et al. (65) show that the fingering does not disappear. In the field, if similar conditions exist, then unstable fingers will form.

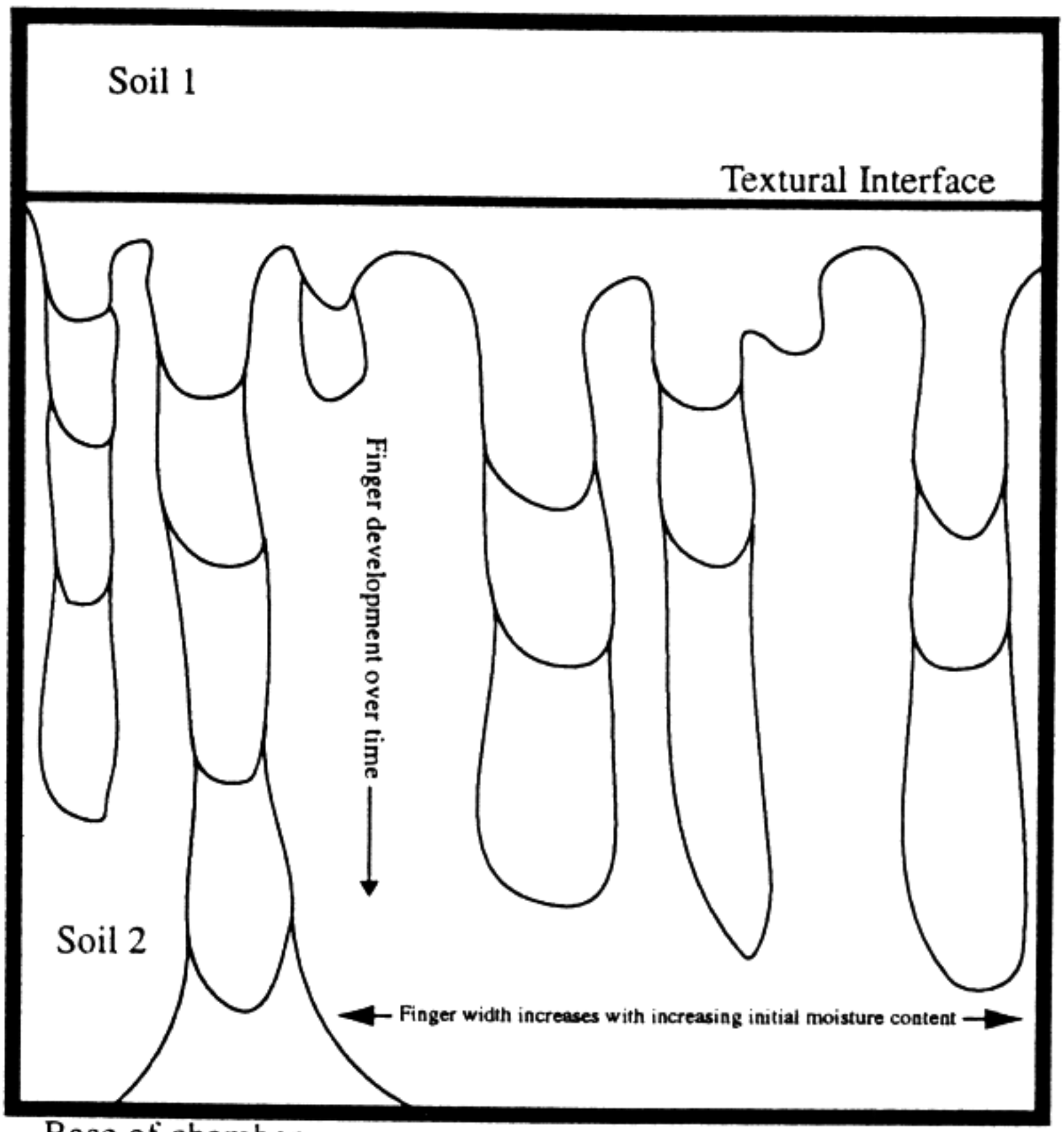

Figure 6. Typical development of fingers (after 59). At the textural interface an instability is established leading to finger formation. The successive lines in the fingers represent the finger location at successive times.

The data from the field experiments of Butters et al. (43) and Ellsworth et al. (45) were analysed quite successfully neglecting any fingering or funnelling. However, the data show the transport vol-

lume changing with depth. These experiments were carried out under a controlled irrigation regime after initial prolonged irrigation to remove profile salts. This suggests that the soil profile was relatively wet, which would tend to broaden any fingers that formed. These authors did note, however, that textural changes in the soil profile did affect the solute movement. Both these mechanisms would cause an apparent nonequilibrium in the solute transport process, as evident in the analyses of Butters et al. (43) and Ellsworth et al. (45). Since the processes involved are much more complicated than in the saturated flow system, in the unsaturated zone it will be more difficult to derive the nondimensional parameter groups controlling the apparent nonequilibrium solute transport. This analysis will not be pursued here (see 67 an illuminating dimensional analysis on the scale of a single finger). However, we suggest that dimensionless analysis similar to that for the saturated flow system can be carried out to help define nonequilibrium solute transport in the unsaturated zone. Possible length scales include the characteristic finger size (68), the distance between fingers, and a soil heterogeneity length scale.

Concluding Remarks

For saturated flow, the mobile-immobile (or two-region) model is the simplest nonequilibrium model available, and many applications suggest that it, or slightly more complicated versions of it, have enough free parameters to model a wide range of solute transport phenomena. However, merely using the model as a fitting tool limits its possible applications. For example, in spite of good fits being obtained, experimental data show that fitted parameters vary with flow velocity, contrary to the common stagnant layer and internal pore diffusion conceptualisations. Dimensional analysis has been used here to help understand the mechanisms leading to nonequilibrium effects. We have suggested that, provided some relatively simple checks are made, it should be possible to scale correctly laboratory results to prototype situations where the flow velocity may be substantially different.

Modelling unsaturated flow and transport using simple models is more difficult due to the effects of heterogeneity and instability. Both of these mechanisms are accentuated compared with saturated flow. The likely net result is that apparent nonequilibrium effects will be increased. Thus, simplified models which do not incorporate a method for simulating nonequilibrium effects will not be particularly useful.

Notation

A	autocorrelation function
BTC	breakthrough curve
c	solute concentration in the liquid phase, ML^{-3}
c_{im}	solute concentration in the immobile liquid phase, ML^{-3}
c_m	solute concentration in the mobile liquid phase, ML^{-3}
d	diffusion/dispersion ratio
D	dispersion coefficient, L^2T^{-1}
Da_I	Damköhler number (Group I)
Da_{II}	Damköhler number (Group II)
Da_{III}	Damköhler number (Group III)
D_{eff}	effective dispersion coefficient derived from the mobile-immobile model, L^2T^{-1}
D_l	local dispersion coefficient, L^2T^{-1}
D_L	effective longitudinal dispersion coefficient, L^2T^{-1}

D_m	molecular diffusion coefficient, L^2T^{-1}
D_M	field scale dispersion coefficient, L^2T^{-1}
f	sorption isotherm, ML^{-3}
K	hydraulic conductivity, LT^{-1}
l	local length scale, L
L	macroscopic length scale, L
l_s	longitudinal correlation length scale for the random velocity field, L
NAPL	nonaqueous phase liquid
P_l	local Péclet number
P_L	macroscopic Péclet number
q, **q**	water flux, LT^{-1}
R	retardation coefficient
s	solute concentration in the solid phase (in liquid phase units), ML^{-3}
t	time, T
t_a	advection time scale, T
t_r	reaction time scale, T
v, **v**	pore water velocity, LT^{-1}
v_s	solute velocity, LT^{-1}
X	length scale ratio
X	particle position, L
z	position, L
α	apparent (sorption) rate constant, T^{-1}
θ	volumetric moisture content
$\bar{\theta}$	depth-averaged moisture content
θ_{im}	immobile liquid volumetric moisture content
θ_m	mobile liquid volumetric moisture content
ν	kinematic viscosity, L^2T^{-1}
σ_v	standard deviation of the random velocity field, LT^{-1}
ϕ	piezometric head, L
Var	variance operator, L^2
∇	del operator, L^{-1}

Literature Cited

1. Feenstra, S., and J. Coburn. 1986. Subsurface contamination from spills of denser than water chlorinated solvents. Calif. WPCA Bull. 23:26-34.
2. Hunt, J. R., N. Sitar, and K. S. Udell. 1988. Nonaqueous phase liquid transport and cleanup. 1. Analysis of mechanisms. Water Resour. Res. 24:1247-1258.
3. Conrad, S. H., J. L. Wilson, W. R. Mason, and W. J. Peplinski. 1992. Visualization of residual organic liquid trapped in aquifers. Water Resour. Res. 28:467-478.
4. Miller, C. T., M. M. Poirier-McNeill, and A. S. Mayer. 1990. Dissolution of trapped nonaqueous phase liquids: Mass transfer characteristics. Water Resour. Res. 26:2783-2796.
5. Powers, S. E., L. M. Abriola, and W. J. Weber. 1992. An experimental investigation of nonaqueous phase liquid dissolution in saturated subsurface systems: Steady state mass transfer rates. Water Resour. Res. 28:2691-2705.
6. Mangold, D. C., and C.-F. Tsang. 1991. A summary of subsurface hydrological and hydrochemical models. Rev. Geophys. 29:51-80.

7. Barry, D. A. 1992. Modelling contaminant transport in the subsurface: Theory and computer programs. In Modelling Chemical Transport in Soil: Natural and Applied Contaminants, H. Ghadiri and C. W. Rose (eds.), Lewis Publishers, Boca Raton, Florida, pp. 105-144.
8. Schweich, D., M. Sardin, and M. Jauzein. 1993. Properties of concentration waves in the presence of nonlinear sorption, precipitation/dissolution, and homogeneous reactions. 1. Fundamentals. Water Resour. Res. 29:723-734.
9. Schweich, D., M. Sardin, and M. Jauzein. 1993. Properties of concentration waves in the presence of nonlinear sorption, precipitation/dissolution, and homogeneous reactions. 2. Illustrative examples. Water Resour. Res. 29:735-742.
10. Jones, M. J., and K. K. Watson. 1987. Effect of soil water hysteresis on solute movement during intermittent leaching. Water Resour. Res. 23:1251-1256.
11. Russo, D., W. A. Jury, and G. L. Butters. 1989. Numerical analysis of solute transport during transient irrigation. 1. The effect of hysteresis and profile heterogeneity. Water Resour. Res. 25:2109-2118.
12. Russo, D., W. A. Jury, and G. L. Butters. 1989. Numerical analysis of solute transport during transient irrigation. 2. The effect of immobile water. Water Resour. Res. 25:2119-2127.
13. Bear, J. 1972. Dynamics of Fluids in Porous Media. Elsevier, New York.
14. Bryant, S. L., R. S. Schechter, and L. W. Lake. 1986. Interactions of precipitation/dissolution waves and ion exchange in flow through permeable media. Am. Inst. Chem. Eng. J. 32:751-764.
15. Sposito, G. 1989. The Chemistry of Soils. Oxford Univ. Press, New York.
16. Sparks, D. L. 1988. Kinetics of Soil Chemical Processes. Academic Press, San Diego.
17. Weber, W. J. 1972. Physiochemical Process for Water Quality Control. Wiley, New York.
18. Weber, W. J., P. M. McGinley, and L. E. Katz. 1991. Sorption phenomena in subsurface systems: Concepts, models and effects on contaminant fate and transport. Water Res. 25:499-528.
19. Benefield, L. D., J. F. Judkins, and B. L. Weand. 1982. Process Chemistry for Water and Wastewater Treatment. Prentice Hall, Englewood Cliffs, New Jersey.
20. Selim, H. M., J. M. Davidson, and R. S. Mansell. 1976. Evaluation of a two-site adsorption-desorption model for describing solute transport in soils. In Proc. of the 1976 Summer Computer Simulation Conference, July, Simulation Councils. La Jolla, Calif.
21. Cameron, D. R., and A. Klute. 1977. Convective-dispersive solute transport with a combined equilibrium and kinetic adsorption model. Water Res. 13:183-188.
22. Coats, K. R., and B. D. Smith. 1964. Dead-end pore volume and dispersion in porous media. Soc. Petrol. Eng. J. 4:73-84.
23. van Genuchten, M. Th. 1981. Non-equilibrium transport parameters from miscible displacement experiments. Res. Rep. No. 119, U. S. Salinity Lab., Riverside, Calif.
24. Nkedi-Kizza, P., J. W. Biggar, M. Th. van Genuchten, P. J. Wierenga, H. M. Selim, J. M. Davidson, and D. R. Nielsen. 1984. On the equivalence of two conceptual models for describing ion exchange during transport through an aggregated oxisol. Water Resour. Res. 20:1123-1130.
25. Boucher, D. F., and G. E. Alves. 1959. Dimensionless numbers. Chem. Eng. Prog. 55:55-64.
26. Herr, M., G. Schäfer, and K. Spitz. 1989. Experimental studies of mass transport in porous media with local heterogeneities. J. Contam. Hydrol. 4:127-137.
27. Li, L., D. A. Barry, P. J. Hensley, and K. Bajracharya. 1993. Nonreactive chemical transport in structured soil: The potential for centrifugal modelling. In R. Fell, T. Phillips and C. Gerrard (eds.), Geotechnical Management of Waste and Contamination, A. A. Balkema, Rotterdam, pp. 425-431.
28. Li, L. 1993. Physical Modelling of Nonreactive Chemical Transport in Locally Inhomogeneous

Soils. M.Eng.Sci. Thesis, Department of Environmental Engineering, Centre for Water Research, University of Western Australia, Nedlands, Western Australia.
29. Parker, J. C., and M. Th. van Genuchten. 1984. Determining Transport Parameters from Laboratory and Field Tracer Experiments. Virginia Agricultural Experiment Station, Bull. 84-3. Blacksburg, Virginia.
30. Saffman, P. G. 1960. Dispersion due to molecular diffusion and macroscopic mixing in flow through a network of capillaries. J. Fluid Mech. 7:194-208.
31. Pfannkuch, H. O. 1963. Contribution a l'étude des déplacements de fluides miscibles dans un mileu poreux. Rev. Inst. Fr. Pétrol. 18:215-270.
32. Sposito, G., and D. A. Barry. 1987. On the Dagan model of solute transport in groundwater: Foundational aspects. Water Resour. Res. 23:1867-1875.
33. Gelhar, L. W., and C. L. Axness. 1983. Three-dimensional stochastic analysis of macrodispersion in aquifers. Water Resour. Res. 19:161-180.
34. Dagan, G. 1987. Theory of solute transport by groundwater. Ann. Rev. Fluid Mech. 19:183-215.
35. Taylor, G. I. 1921. Diffusion by continuous movements. Proc. Lond. Math. Soc. 20:196-211.
36. Barry, D. A., and G. Sposito. 1989. Analytical solution of a convection-dispersion model with time-dependent transport coefficients. Water Resour. Res. 25:2407-2416.
37. Gelhar, L. W., C. Welty, and K. R. Rehfeldt. 1992. A critical review of data on field-scale dispersion in aquifers. Water Resour. Res. 28:1955-1974.
38. Kung, K.-J. S. 1990. Preferential flow in a sandy vadose zone: 1. Field observation. Geoderma 46:51-58.
39. Kung, K.-J. S. 1990. Preferential flow in a sandy vadose zone: 2. Mechanism and implications. Geoderma 46:59-71.
40. Biggar, J. W., and D. R. Nielsen. 1976. Spatial variability of the leaching characteristics of a field soil. Water Resour. Res. 12:78-84.
41. van de Pol, R. M., P. J. Wierenga, and D. R. Nielsen. 1977. Solute movement in a field soil. Soil Sci. Soc. Am. J. 41:10-13.
42. Wild, A., and I. A. Babiker. 1976. The asymmetric leaching pattern of nitrate and chloride in a loamy sand under field conditions. J. Soil Sci. 27:460-466.
43. Butters, G. L., W. A. Jury, and F. F. Ernst. 1989. Field scale transport of bromide in an unsaturated soil. 1. Experimental methodology and results. Water Resour. Res. 25:1575-1581.
44. Butters, G. L., and W. A. Jury. 1989. Field scale transport of bromide in an unsaturated soil. 2. Dispersion modeling. Water Resour. Res. 25:1583-1589.
45. Ellsworth, T. R., W. A. Jury, F. F. Ernst, and P. J. Shouse. 1991. A three-dimensional field study of solute transport through unsaturated, layered, porous media. 1. Methodology, mass recovery, and mean transport. Water Resour. Res. 27:951-965.
46. Ellsworth, T. R., and W. A. Jury. 1991. A three-dimensional field study of solute transport through unsaturated, layered, porous media. 2. Characterization of vertical dispersion. Water Resour. Res. 27:967-981.
47. White, R. E., J. Dyson, R. A. Haigh, W. A. Jury, and G. Sposito. 1986. Transfer function model of solute transport through soil. 2. Illustrative applications. Water Resour. Res. 22:248-254.
48. Saffman, P. G., and G. Taylor. 1958. The penetration of a fluid into a porous media or Hele-Shaw cell containing a more viscous fluid. Proc. R. Soc. London, Ser. A. 245:312-329.
49. Chuoke, R. L., P. van Meurs, and C. van del Poel. 1959. The instability of slow immiscible, viscous liquid-liquid displacements in porous media. Trans. Am. Inst. Min. Metall. Pet. Eng. 216:188-194.

50. Rachford, H. H. 1964. Instability of water flooding oil from water-wet porous media containing connate water. Soc. Pet. Eng. J. 4:133-148.
51. Hill, D. E., and J.-Y. Parlange. 1972. Wetting front instability in layered soils. Soil Sci. Soc. Am. Proc. 36:697-702.
52. Parlange, J.-Y., and D. E. Hill. 1976. Theoretical analysis of wetting front instability in soils. Soil Sci. 122:236-239.
53. Philip, J. R. 1975. Stability analysis of infiltration. Soil Sci. Soc. Am. Proc. 39:1042-1049.
54. Raats, P. A. C. 1973. Unstable wetting fronts in uniform and non-uniform soils. Soil Sci. Soc. Am. Proc. 36:681-685.
55. White, I., P. M. Colombera, and J. R. Philip. 1976. Experimental studies of wetting front instability induced by sudden changes of pressure gradient. Soil Sci. Soc. Am. Proc. 40:824-829.
56. White, I., P. M. Colombera, and J. R. Philip. 1977. Experimental studies of wetting front instability induced by gradual changes of pressure gradient and by heterogeneous porous media. Soil Sci. Soc. Am. Proc. 41:483-489.
57. Diment, G. A., K. K. Watson, and P. J. Blennerhassett. 1982. Stability analysis of water movement in unsaturated porous materials. 1. Theoretical considerations. Water Resour. Res. 18:1248-1254.
58. Diment, G. A., and K. K. Watson. 1983. Stability analysis of water movement in unsaturated porous materials. 2. Numerical studies. Water Resour. Res. 19:1002-1010.
59. Diment, G. A., and K. K. Watson. 1985. Stability analysis of water movement in unsaturated porous materials. 3. Experimental studies. Water Resour. Res. 21:979-984.
60. Glass, R. J., T. S. Steenhuis, and J.-Y. Parlange. 1988. Wetting front instability as a rapid and far-reaching hydrologic process in the vadose zone. J. Contam. Hydrol. 3:207-226.
61. Glass, R. J., T. S. Steenhuis, and J.-Y. Parlange. 1989. Mechanism for finger persistence in homogeneous, unsaturated, porous media: Theory and verification. Soil Sci. 148:60-70.
62. Glass, R. J., S. Cann, J. King, N. Bailey, J.-Y. Parlange, and T. S. Steenhuis. 1990. Wetting front instability in unsaturated porous media: A three-dimensional study. Transp. Porous Media 5:247-268.
63. Selker, J., P. Leclerq, J.-Y. Parlange, and T. S. Steenhuis. 1992. Fingered flow in two dimensions. 1. Measurement of matric potential. Water Resour. Res. 28:2513-2521.
64. Selker, J., J.-Y. Parlange, and T. S. Steenhuis. 1992. Fingered flow in two dimensions. 2. Predicting finger moisture profile. Water Resour. Res. 28:2523-2528.
65. Glass, R. J., T. S. Steenhuis, and J.-Y. Parlange. 1989. Wetting front instability. 2. Experimental determination of relationships between system behavior in initially dry porous media. Water Resour. Res. 25:1195-1207.
66. Starr, J. L., H. C. DeRoo, R. Frink, and J.-Y. Parlange. 1978. Leaching characteristics of a layered field soil. Soil Sci. Soc. Am. J. 42:386-391.
67. Glass, R. J., T. S. Steenhuis, and J.-Y. Parlange. 1989. Wetting front instability. 1. Theoretical discussion and dimensional analysis. Water Resour. Res. 25:1187-1194.
68. Glass, R. J., J.-Y. Parlange, and T. S. Steenhuis. 1991. Immiscible displacement in porous media: Stability analysis of three-dimensional, axisymmetric disturbances with application to gravity-driven wetting front instability. Water Resour. Res. 27: 1947-1956.